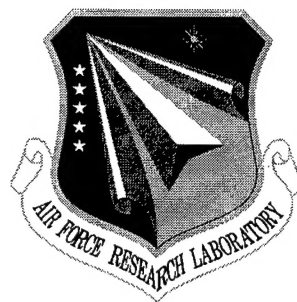


AFRL-SN-RS-TR-1998-182

Final Technical Report

September 1998



EFFECTS OF ANTENNA MUTUAL COUPLING IN SPACE-TIME ADAPTIVE PROCESSING (STAP)

Research Associates for Defense Conversion, Inc.

Braham Himed

APPROVED FOR PUBLIC RELEASE; DISTRIBUTION UNLIMITED.

19990107 014


**AIR FORCE RESEARCH LABORATORY
SENSORS DIRECTORATE
ROME RESEARCH SITE
ROME, NEW YORK**

Although this report references a limited document (*), listed on page 29, no limited information has been extracted.

This report has been reviewed by the Air Force Research Laboratory, Information Directorate, Public Affairs Office (IFOIPA) and is releasable to the National Technical Information Service (NTIS). At NTIS it will be releasable to the general public, including foreign nations.

AFRL-SN-RS-TR-1998-182 has been reviewed and is approved for publication.

APPROVED:


JAMES H. MICHELS
Project Engineer

FOR THE DIRECTOR:



ROBERT G. POLCE, Acting Chief
Rome Operations Office
Sensors Directorate

If your address has changed or if you wish to be removed from the Air Force Research Laboratory Rome Research Site mailing list, or if the addressee is no longer employed by your organization, please notify AFRL/SNRT, 26 Electronic Pky, Rome, NY 13441-4514. This will assist us in maintaining a current mailing list.

Do not return copies of this report unless contractual obligations or notices on a specific document require that it be returned.

REPORT DOCUMENTATION PAGE			Form Approved OMB No. 0704-0188	
<small>Public reporting burden for this collection of information is estimated to average 1 hour per response, including the time for reviewing instructions, searching existing data sources, gathering and maintaining the data needed, and completing and reviewing the collection of information. Send comments regarding this burden estimate or any other aspect of this collection of information, including suggestions for reducing this burden, to Washington Headquarters Services, Directorate for Information Operations and Reports, 1215 Jefferson Davis Highway, Suite 1204, Arlington, VA 22202-4302, and to the Office of Management and Budget, Paperwork Reduction Project (0704-0188), Washington, DC 20503.</small>				
1. AGENCY USE ONLY (Leave blank)	2. REPORT DATE September 1998	3. REPORT TYPE AND DATES COVERED Final May 96 - Oct 97		
4. TITLE AND SUBTITLE EFFECTS OF ANTENNA MUTUAL COUPLING IN SPACE-TIME ADAPTIVE PROCESSING (STAP)		5. FUNDING NUMBERS C - F30602-96-C-0110 PE - 61102F PR - 2300 TA - 06 WU - PO		
6. AUTHOR(S) Braham Himed				
7. PERFORMING ORGANIZATION NAME(S) AND ADDRESS(ES) Research Associates for Defense Conversion, Inc. 10002 Hillside Terrace Marcy NY 13403		8. PERFORMING ORGANIZATION REPORT NUMBER N/A		
9. SPONSORING/MONITORING AGENCY NAME(S) AND ADDRESS(ES) AFRL/SNRT 26 Electronic Pky Rome NY 13441-4514		10. SPONSORING/MONITORING AGENCY REPORT NUMBER AFRL-SN-RS-TR-1998-182		
11. SUPPLEMENTARY NOTES AFRL Project Engineer: James H. Michels/SNRT/(315) 330-4432				
12a. DISTRIBUTION AVAILABILITY STATEMENT Approved for public release; distribution unlimited.		12b. DISTRIBUTION CODE		
13. ABSTRACT (Maximum 200 words) This report considers the impact of antenna mutual coupling on adaptive phased array radar signal processing. First, the impedance matrix is developed via the method of moments and utilized in an airborne phased array radar data generation code. Next, the effect of mutual coupling on the true and estimated covariance matrices is considered. Finally, performance results are considered for a space-time adaptive processing algorithm in terms of probability of detection as well as plots of the test statistics versus angle-doppler.				
14. SUBJECT TERMS Mutual Coupling, Space-Time Adaptive Processing, Radar Signal Processing		15. NUMBER OF PAGES 40		
		16. PRICE CODE		
17. SECURITY CLASSIFICATION OF REPORT UNCLASSIFIED	18. SECURITY CLASSIFICATION OF THIS PAGE UNCLASSIFIED	19. SECURITY CLASSIFICATION OF ABSTRACT UNCLASSIFIED	20. LIMITATION OF ABSTRACT UL	

Table of Contents

1. Introduction	1
2. Model	2
3. Modification of the Physical Model	6
4. Application to Space Time Adaptive Processing	16
5. Effects of Mutual Coupling on the True SINR	20
6. Probability of Detection	21
7. Conclusions and Recommendations for Future Work	28
References	29

List of Figures

Figure 1. Sub-sectioning of the J dipoles	2
Figure 2. Real part of true temporal covariance sequence for channel	9
Figure 3. Imaginary part of true temporal covariance sequence for channel	10
Figure 4. Real part of temporal sample covariance estimate	11
Figure 5. Imaginary part of temporal sample covariance estimate	11
Figure 6. Real part of spatial true covariance sequence	12
Figure 7. Imaginary part of spatial true covariance sequence	13
Figure 8. Real part of spatial sample covariance estimate	14
Figure 9. Imaginary part of spatial sample covariance estimate	14
Figure 10. Normalized true power spectrum	15
Figure 11. Normalized true power spectrum	15
Figure 12. Normalized true power spectrum (modified periodogram)	16
Figure 13. Estimated SINR, without, with and compensating for mutual coupling.	18
Figure 14. Adapted pattern, without, with and compensating for mutual coupling.	19
Figure 15. Test statistic, without, with and compensating for mutual coupling.	19
Figure 16. Pd vs. SNR, J = 2, N = 2, K = 1000	22
Figure 17. Pd vs. SNR, J = 2, N = 2, K = 8	23
Figure 18. Pd vs. elevation angle θ	24
Figure 19. Pd vs. Normalized Doppler Frequency, $\theta = 0^\circ$	25
Figure 20. Pd vs. Normalized Doppler Frequency, $\theta = 30^\circ$	26
Figure 21. Pd vs. Normalized Doppler Frequency, $\theta = 60^\circ$	27
Figure 22. Pd vs. SNR, J = 4, N = 8, K = 64	28

List of Tables

Table 1. SINR as a function of n , no mutual coupling	21
Table 2. SINR as a function of n , with mutual coupling	21

1. Introduction

In most signal processing techniques, the elements of a sensor array are treated as independent entities. However, in practice, mutual coupling exists between the array sensors. Because the mutuals change the sensor impedances, the gain and radiation pattern of the array can be greatly distorted. Gupta and Ksienski [1] investigated the effects of mutual coupling on the performance of an adaptive array. In their treatment, the matrix Z_0 characterizing the mutual coupling between the sensors was determined using a mathematical model which models the antenna array consisting of J sensors as an $(J + 1)$ terminal network. This matrix was then used to determine the sensor outputs that would have existed had there been no mutual coupling. A compensation scheme was then developed to study the performance of the conventional beamforming technique. Yeh and Leou [2] used the same mathematical model and applied it to the MUSIC algorithm. Recall, in the MUSIC algorithm, that one plots the inverse of the correlation between the noise subspace E_n and the directional vector $a(\theta)$, which we denote by $\left[\|E_n a(\theta)\|^2\right]^{-1}$. If mutual coupling is present, Yeh and Leou show that one has to plot the function $\left[\|E_n Z_0^{-1} a(\theta)\|^2\right]^{-1}$. Failure to do so results in severe degradation of the estimates. Shau [3] considered the case of deterministic signals in a noise free environment and eliminated the effects of mutual coupling for the method known as the Modified Forward Backward Linear Prediction (MFBLP). Himed [4] considered the case of mutual coupling for narrowband signals and effectively compensated for the effects of mutual coupling for the techniques known as the Matrix Pencil Approach, with two different operators, namely the Moving Window and ESPRIT. Two recent analyses [6,7] have also considered the effects of mutual coupling. In [6], the performance of high-resolution direction finding systems such as MUSIC is studied under a wideband scenario. They show that performance is adversely affected by mutual coupling not only at the low end of the frequency band but also at the high end. They devised ways to correct the actual voltage matrix using the terminal impedance matrix that is derived from the MOM impedance matrix. Their results approach the ideal case. However, this correction does not involve the alteration of the signal-processing algorithm. In [7], an adaptive algorithm that accounts for the mutual coupling between the elements of an array was studied. It is shown that failure to

account for mutual coupling causes the failure of all adaptive techniques. Their technique is based again on the MOM admittance matrix to quantize the mutual coupling and to find the optimum weights to produce the desired nulling.

In this effort we develop algorithms to effectively compensate for the effects of mutual coupling when using space-time adaptive processing techniques. However, for simplicity, we will only use the model described in [4]. The next section describes the proposed model.

2. Model

We restrict ourselves to a simple model and consider a linear array of J dipoles uniformly spaced at a distance d . Each dipole is of length t and has a radius r satisfying the condition $r \ll t$. A load is attached to the center gap of each dipole. Assume there are q narrowband signals impinging on the array as planar wavefronts. The voltages induced by the assumed signals on the loads are the outputs of the dipoles. Induced currents will appear on the dipoles. These currents reradiate and generate scattered fields. The scattered fields then induce currents on the neighboring dipoles. The process of induction and reradiation causes the mutual coupling among the dipoles.

Using one sinusoidal expansion and weighting function per dipole, the method of moments [5] was used to obtain the matrix of mutuals (see Figure 1).

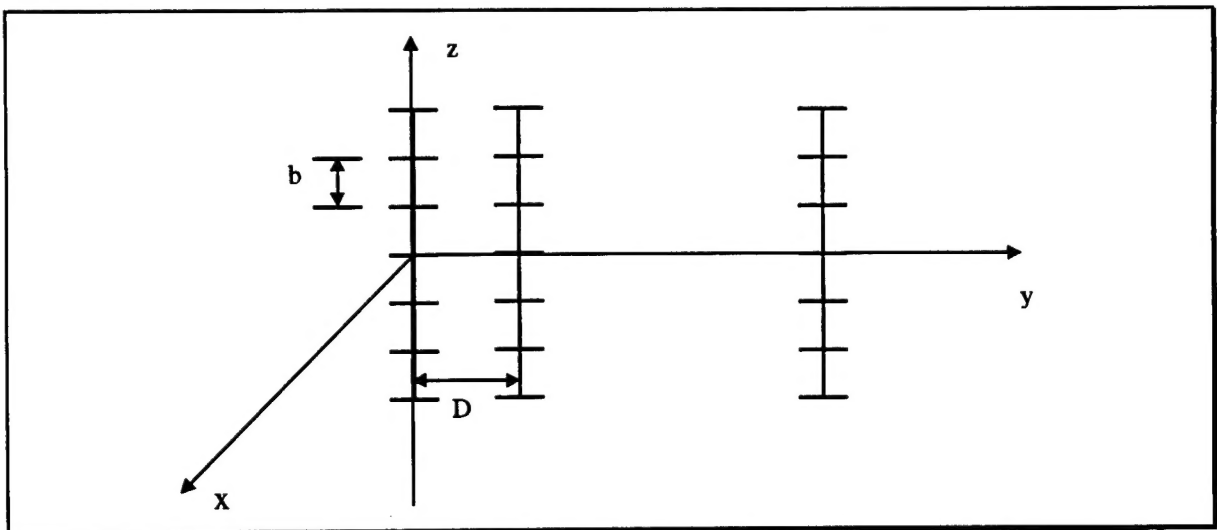


Figure 1. Sub-sectioning of the J dipoles.

Denote the current distribution by $\kappa(z)$, (assuming longitudinal distribution and neglecting all other distributions) and the i -th expansion function by $f_i(z)$. Then

$$\kappa(z) = \sum_{i=1}^J I(i) f_i(z) \quad (1)$$

where $I(i)$; $i=1,2,\dots,J$, denotes the unknown current amplitude to be determined on each dipole. At a point (y,z) in the $Y-Z$ plane, the scattered field is given by

$$E^{(s)}(y,z) = \sum_{i=1}^J I(i) E_i^{(s)}(y,z) \quad (2)$$

where $E^{(s)}(y,z)$ is the scattered field from the i -th dipole. The total field will then be

$$E(y,z) = E^{(inc)}(y,z) + E^{(s)}(y,z) \quad (3)$$

where $E^{(inc)}$ is the incident field. Let E_z be the z -component of the total field. A generalized voltage $V(k)$ induced on the subsection spanned by the function $f_k(z)$ can be defined with respect to a weighting function $w_k(z)$ as

$$V(k) = F[E_z(y,z), w_k(z)] \quad (4)$$

where $F(.,.)$ is bilinear with respect to $E_z(y,z)$ and $w_k(y,z)$. Similarly, we define the voltage produced by the incident field on the k -th dipole by

$$V^{(inc)}(k) = F[E_z^{(inc)}(y,z), w_k(z)] \quad (5)$$

and the voltage produced by the scattered field on the k -th dipole by

$$V^{(s)}(k) = F[E_z^{(s)}(y,z), w_k(z)]. \quad (6)$$

Thus, the total voltage introduced in the k -th dipole is

$$V(k) = V^{(inc)}(k) + V^{(s)}(k), \quad (7)$$

which, for metallic scatterers, becomes

$$V(k) = V^{(inc)}(k) + V^{(s)}(k) = 0 \quad (8)$$

or

$$V^{(inc)}(k) = -V^{(s)}(k). \quad (9)$$

However,

$$\underline{V}^{(s)}(k) = F \left[\sum_{i=1}^J I(i) E_i^{(s)}(y, z), w_k(z) \right] = \sum_{i=1}^J I(i) F[E_i^{(s)}(y, z), w_k(z)]. \quad (10)$$

The total impedance between the k-th and i-th dipoles is defined to be

$$z^{ki} = -F[E_i^{(s)}(y, z), w_k(z)]. \quad (11)$$

Thus,

$$\underline{V}^{(s)}(k) = \sum_{i=1}^J -z^{ki} I(i) \quad ; \quad k = 1, 2, \dots, J. \quad (12)$$

In matrix notation

$$\underline{V}^{(s)} = -Z \underline{I} \quad (13)$$

where

$$\underline{V}^{(s)} = [V^{(s)}(1) \ , \ V^{(s)}(2) \ , \ \dots \ , \ V^{(s)}(J)]^T \quad (14)$$

and

$$\underline{I} = [I(1) \ , \ I(2) \ , \ \dots \ , \ I(J)]^T. \quad (15)$$

The total impedance matrix Z can be decomposed into two parts as

$$Z = Z_0 + Z_L \quad (16)$$

where, Z_0 is the generalized impedance matrix and Z_L is the load matrix.

Assuming that all loads are loaded with the same load z_l , the matrix Z_L is a diagonal matrix with elements z_l and is given by

$$Z_L = \text{diag}(z_l). \quad (17)$$

The ki -th element of Z , therefore, is

$$z^{ki} = z_{ki} + z_l \delta_{ki}, \quad (18)$$

where z_{ki} is the mutual impedance between the k-th and i-th dipoles. The total voltages induced on a load z_l are given by

$$\underline{V}^{(L)} = Z_L \underline{I} \quad \text{and} \quad \underline{I} = Z_L^{-1} \underline{V}^{(L)}. \quad (19)$$

However,

$$\underline{V}^{(inc)} = Z \underline{I} = Z_0 Z_L^{-1} \underline{V}^{(L)} + \underline{V}^{(L)} = (I + Z_0 Z_L^{-1}) \underline{V}^{(L)}, \quad (20)$$

which implies that

$$\underline{V}^{(L)} = (\underline{I} + \underline{Z}_0 \underline{Z}_L^{-1})^{-1} \underline{V}^{(inc)}. \quad (21)$$

Let \underline{H} be the matrix

$$\underline{H} = (\underline{I} + \underline{Z}_0 \underline{Z}_L^{-1}). \quad (22)$$

\underline{H} can be written as

$$\underline{H} = \begin{bmatrix} 1 + (z_{11}/z_1) & (z_{12}/z_1) & \cdots & (z_{1J}/z_1) \\ (z_{21}/z_1) & 1 + (z_{22}/z_1) & \cdots & (z_{2J}/z_1) \\ \vdots & \vdots & \vdots & \vdots \\ (z_{J1}/z_1) & (z_{J2}/z_1) & \cdots & 1 + (z_{JJ}/z_1) \end{bmatrix}. \quad (23)$$

Thus, when incident signals are impinging on the array and in the presence of additive noise, the output of the linear array, at time n , will be

$$\underline{V}^{(L)}(n) = \underline{H}^{-1} \underline{V}^{(inc)}(n) + \underline{w}(n), \quad n = 1, 2, \dots, N \quad (24)$$

where N is the number of pulses and $\underline{w}(n)$ is the additive white noise vector.

Note that usually, the vector $\underline{V}^{(inc)}(n)$ consists of signal vectors, clutter and jamming signals.

The problem, therefore, becomes one of accounting for mutual coupling in the data generation and ways to compensate for these effects in the signal processing stage.

Of particular interest to us is a signal generation code developed by Scientific Studies Corporation (SSC) for airborne radar applications [8]. This data generation technique is being used in the Air Force Research Laboratory Multi-Channel Signal Processing System (AFRL-MCSPS). In the remainder of this report, we will refer to this section of the code as the physical model.

The physical model is a very powerful tool for signal generation, especially for algorithm evaluation and comparison. It provides the user with both a datacube consisting of J channels, N pulses and K range cells, and the true covariance matrices of all components involved in the simulation (target, clutter and jamming). This allows for optimal performance evaluation of STAP algorithms. However, for our purposes, we modified the code so as to generate the space-time true covariance matrices as well as estimates of these matrices generated using the sample covariance matrix.

3. Modification of the Physical Model

The first task in this effort is to incorporate the effects of mutual coupling into the MCSPS's physical model (data generation). Therefore, care must be taken to incorporate these effects into all of the signals involved in the simulation, i.e.; target, clutter and jamming.

Note that the physical model [8] enables the user to generate a sequence of data as well as the "true covariance" matrices of the involved signals [8]. First, we made changes to the code so that the output sequence will be available to the user with each component identified separately. This is desired for diagnostics purposes.

A MATLAB code was written to compute the matrix of mutuals. This was done for the case of a linear uniformly spaced array composed of half-wavelength dipoles as described in section 2. The load impedance z_L was assumed to be z_{11}^* . This then was incorporated into the physical model and the user can now generate space-time data with the effects of mutual coupling included in the data generation. At this stage, the matrix of mutuals is applied to all data vectors, however, it is also possible for the user to choose which data sets (i.e.; targets, jammers or clutter) the matrix of mutuals will be applied to.

To illustrate this, consider the following signal vector \underline{s} , usually given by

$$\underline{s} = a(\underline{s}_t \otimes \underline{s}_s), \quad (25)$$

where a is a constant (complex) amplitude, \underline{s}_t is a temporal steering vector, \underline{s}_s is a spatial steering vector and \otimes denotes the Kronecker tensor product. In the presence of mutual coupling, only the spatial steering vector is affected and is then modified as follows

$$\underline{s}_{s,z} = H^{-1} \underline{s}_s. \quad (26)$$

The new signal vector \underline{s}_z then becomes

$$\underline{s}_z = a(\underline{s}_t \otimes \underline{s}_{s,z}) = a[\underline{s}_t \otimes (H^{-1} \underline{s}_s)]. \quad (27)$$

A similar operation is applied to all signal vectors including target, clutter and jamming. This does not affect additive white noise.

Consider now the received space-time vector, which we denote by \underline{X} . \underline{X} can be written as

$$\underline{X}^T = [\underline{x}(1) \quad \underline{x}(2) \quad \dots \quad \underline{x}(N)], \quad (28)$$

where the vector $\underline{x}(n)$; $n=1,2,\dots,N$, is a composite of target signal, clutter, jamming and additive white noise. It is generally given as

$$\underline{x}(n) = \underline{t}(n) + \underline{c}(n) + \underline{i}(n) + \underline{w}(n) ; n = 1, 2, \dots, N \quad (29)$$

where $\underline{t}(n)$ is the target signal vector, $\underline{c}(n)$ is the clutter signal vector, $\underline{i}(n)$ is the jamming signal vector and the $\underline{w}(n)$ is the additive white Gaussian noise assumed to be independent and identically distributed.

In the absence of mutual coupling, the covariance matrix of the received signal vector \underline{X} is given by

$$R_x = E\{\underline{X}\underline{X}^H\} = R_t + R_c + R_i + R_n, \quad (30)$$

where R_t , R_c , R_i and R_n are the covariance matrices of the target, clutter, jamming and noise, respectively.

To further simplify our analysis, we assume that the datacube consists of J channels, N pulses and K range cells. For simplicity, let \underline{y} denote a general vector used to denote any specific process, \underline{t} , \underline{c} , or \underline{i} . The received space-time vector \underline{y} has therefore dimension $JN \times K$. Each column of \underline{y} is assumed to have been formed by concatenating all channels for pulse 1 through pulse N . Let $\underline{y}(n)$ be the $J \times 1$ signal vector obtained at pulse n .

$$\underline{y}^T(n) = [y_1(n) \quad y_2(n) \quad \dots \quad y_J(n)], \quad (31)$$

where $y_k(n)$ is the signal received at the k -th channel and n -th pulse. Then, the space-time vector \underline{Y} can be expressed as (in concatenated form)

$$\underline{Y}^T = [\underline{y}(1) \quad \underline{y}(2) \quad \dots \quad \underline{y}(N)]. \quad (32)$$

In the presence of mutual coupling, the vector $\underline{y}_z(n)$ replaces the vector $\underline{y}(n)$, where $\underline{y}_z(n)$ is given by

$$\underline{y}_z(n) = H^{-1} \underline{y}(n) ; n = 1, 2, \dots, N. \quad (33)$$

The received space-time vector is then changed to

$$\underline{Y}_z^T = \{\underline{y}_z(1) \quad \underline{y}_z(2) \quad \dots \quad \underline{y}_z(N)\} = \{H^{-1} \underline{y}(1) \quad H^{-1} \underline{y}(2) \quad \dots \quad H^{-1} \underline{y}(N)\}. \quad (34)$$

Let Γ be the following matrix

$$\Gamma = \text{diag}(\mathbf{H}^{-1}) = \begin{bmatrix} \mathbf{H}^{-1} & 0 & \dots & 0 \\ 0 & \mathbf{H}^{-1} & \dots & 0 \\ \vdots & \vdots & \dots & \vdots \\ 0 & 0 & \dots & \mathbf{H}^{-1} \end{bmatrix}. \quad (35)$$

Then $\underline{\mathbf{Y}}_z$ can be expressed as

$$\underline{\mathbf{Y}}_z = \Gamma \underline{\mathbf{Y}}. \quad (36)$$

Hence, in the presence of mutual coupling, the received signal vector is expressed as

$$\underline{\mathbf{x}}_x(n) = \mathbf{H}^{-1} [\underline{\mathbf{t}}(n) + \underline{\mathbf{c}}(n) + \underline{\mathbf{i}}(n)] + \underline{\mathbf{w}}(n); \quad n = 1, 2, \dots, N,$$

and the concatenated space-time vector can be written as

$$\underline{\mathbf{X}}_z = \Gamma \underline{\mathbf{X}} + \underline{\mathbf{W}}, \quad (37)$$

where $\underline{\mathbf{W}}$ is the space-time additive white noise vector. Thus, the received signal (target, clutter, jamming + noise) covariance matrix is given by

$$\mathbf{R}_{x,z} = E\{\underline{\mathbf{X}}_z \underline{\mathbf{X}}_z^H\} = \Gamma (\mathbf{R}_t + \mathbf{R}_c + \mathbf{R}_i) \Gamma^H + \mathbf{R}_w. \quad (38)$$

Therefore, in the presence of mutual coupling, Equations (37) and (38) are used throughout the simulation code.

For diagnostics purposes, we applied the matrix of mutuals to each component (target, jamming and clutter) individually and made all signal components available to the user. We have also included the effects of the mutual coupling on the true covariance matrices of the targets, jamming and clutter, as described by Equation (38).

We now illustrate the impact of mutual coupling upon both the true covariance matrix as well as the sample matrix estimator defined as

$$\hat{\mathbf{R}} = \frac{1}{K} \sum_{k=1}^K \underline{\mathbf{X}}_k \underline{\mathbf{X}}_k^H, \quad (39)$$

where $\underline{\mathbf{X}}_k$ is the space-time composite signal (target, clutter, jamming and noise) vector. Let \mathbf{R} be the true covariance matrix.

We consider a simulation for a linear array consisting of $J = 14$ channels uniformly spaced at $d = (\lambda/2)$ and a coherent processing interval (CPI) of $N = 18$ pulses. A pulse

repetition frequency (PRF) of 300 Hz is assumed and a 450 MHz transmit frequency is used. In the scenario, we had a target, two jammers, clutter and additive white noise.

Figures 2 and 3 show the output of the real and imaginary part, respectively, of the true channel 1 temporal covariance sequence without and with mutual coupling as a function of the temporal lag. This sequence is obtained from the (1,1) element of each $J \times J$ block matrix contained in the first block row of the $JN \times JN$ covariance matrix.

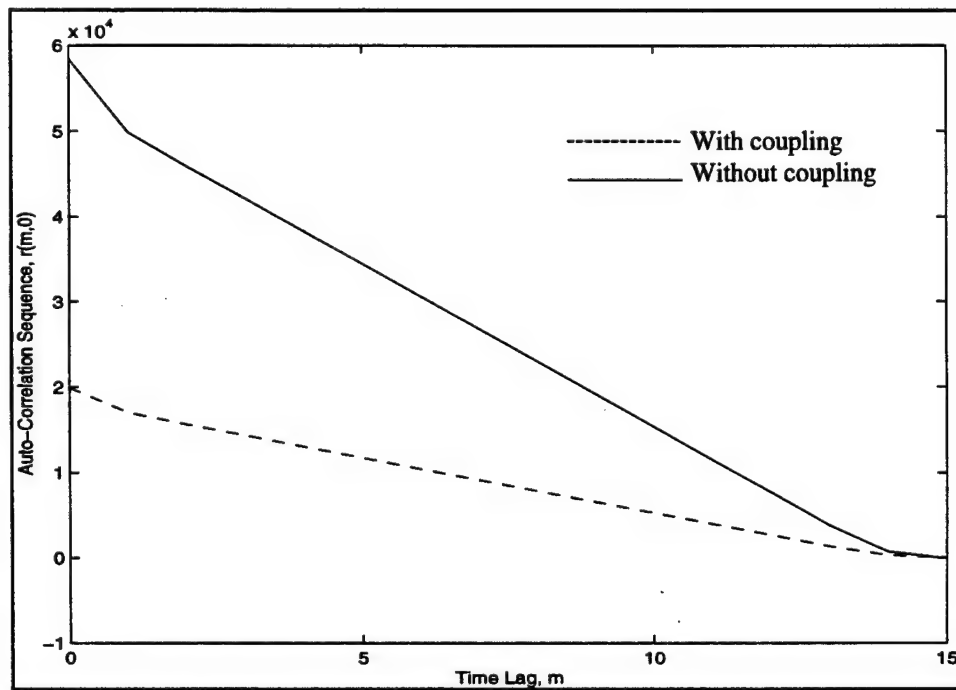


Figure 2. Real part of true temporal covariance sequence for channel 1.

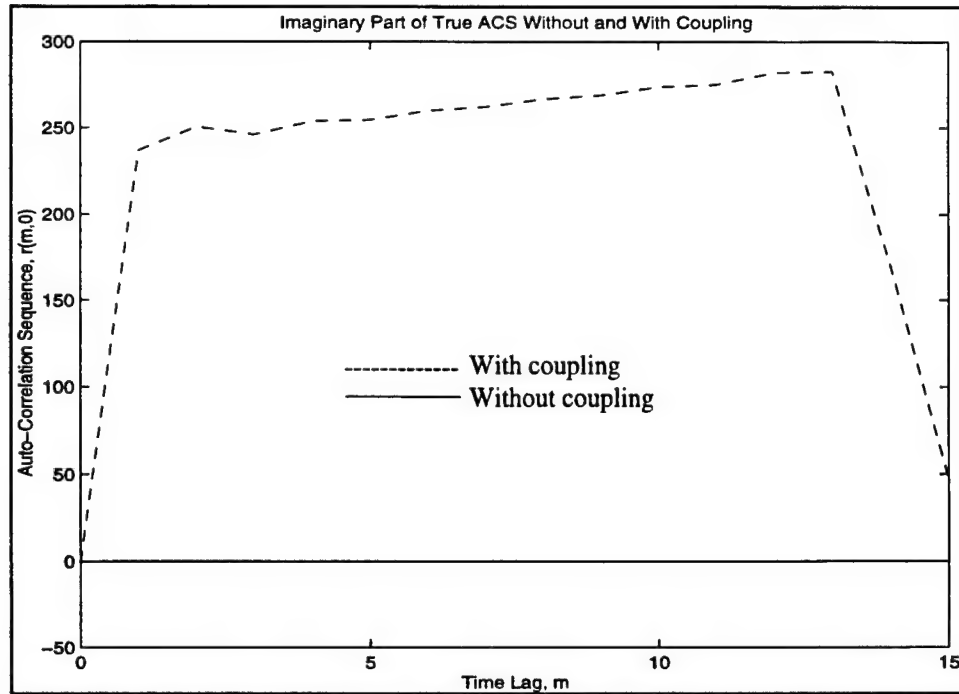


Figure 3. Imaginary part of true temporal covariance sequence for channel 1.

From Figures 2 and 3, note that mutual coupling does change the true temporal covariance sequence. The change is more accentuated in the imaginary part. Even though, mutual coupling affects the spatial component of the covariance matrix, the pre- and post-multiplications by the matrix of mutuals of the space-time covariance matrix do affect the temporal aspect of the matrix.

Figures 4 and 5 show the output of the real and imaginary part of the sample covariance matrix, estimated from 448 secondary data cells.

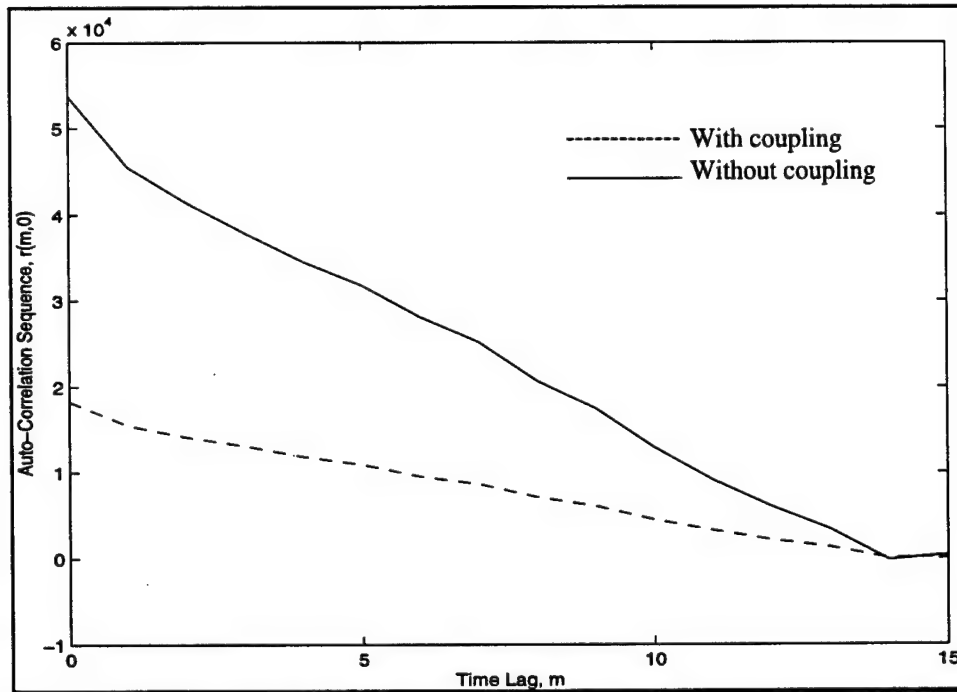


Figure 4. Real part of temporal sample covariance sequence.

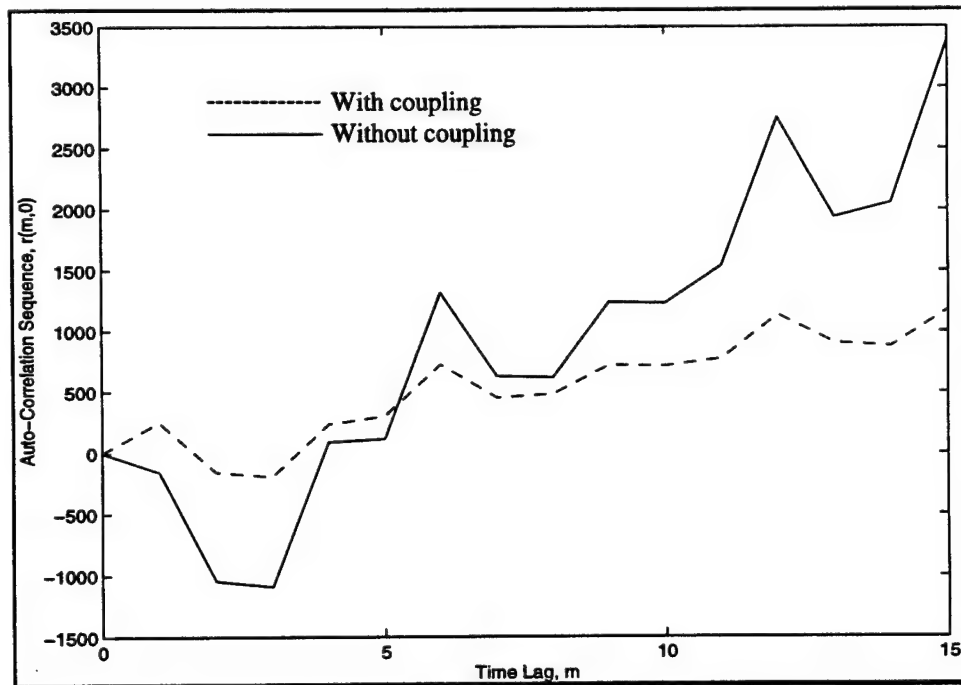


Figure 5. Imaginary part of temporal sample covariance sequence.

As noted in Figures 4 and 5, mutual coupling also affects the sample covariance matrix estimator. This is expected since the matrix of mutuals affects the sample covariance

matrix in the same manner as the true covariance matrix. The differences between the true and estimated values are due to the small sample support size (K) used in the estimation procedure of Equation (39).

Figures 6 and 7 show the spatial variations of the real and imaginary parts, respectively, of the true space-time covariance matrix with and without mutual coupling. In these figures, we plot the cross-channel correlation sequence as a function of the spatial lag (i.e., the integer difference between the channel numbers) with channel 1 used as the reference channel). We emphasize, however, that spatial stationarity does not hold in the presence of mutual coupling between elements. Therefore, we would expect variations in the cross-channel correlation sequence when using another channel as the reference channel.

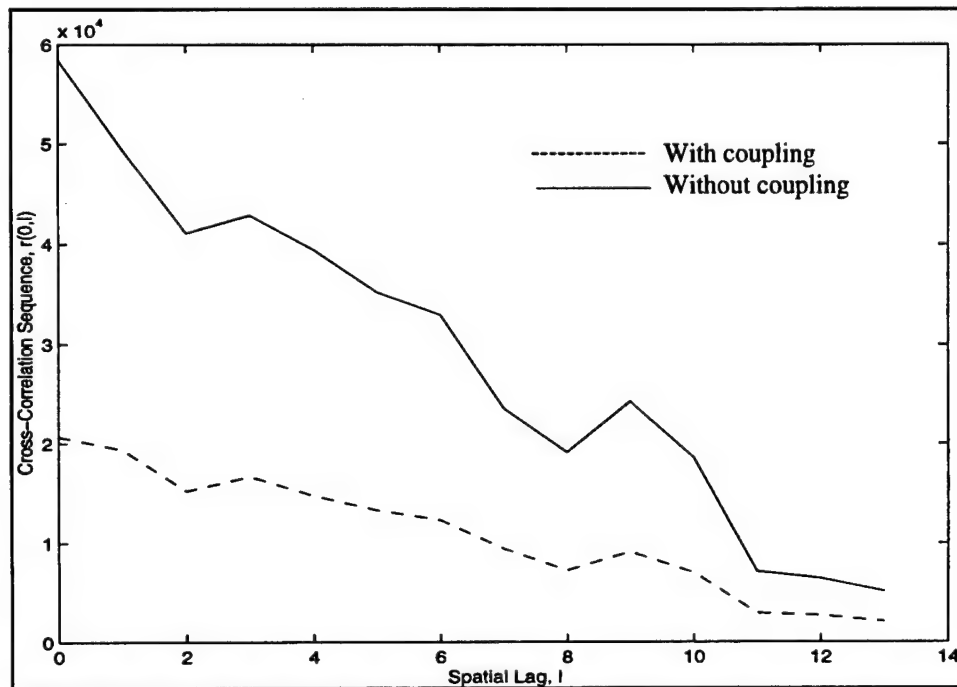


Figure 6. Real part of true spatial covariance sequence.

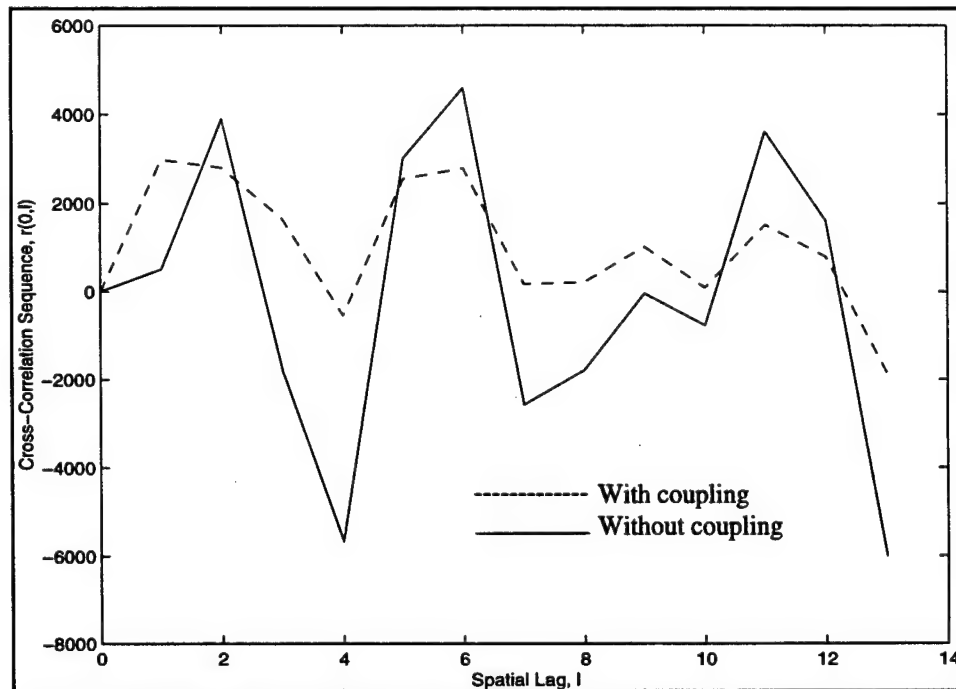


Figure 7. Imaginary part of true spatial covariance sequence.

Figures 6 and 7 are important because they clearly show the effects of mutual coupling. As we have stated earlier, mutual coupling affects the spatial variation aspect of both the received signal vector as well as its true covariance matrix. This shows very clearly in both figures as the real and imaginary components of the true covariance matrix deviate from their values when mutual coupling is included.

Figures 8 and 9 show the real and imaginary parts of the estimated sample covariance matrix. The procedure used here is described in the MATLAB code given above. For simplicity, only the first J terms of the first column are used in the simulation.

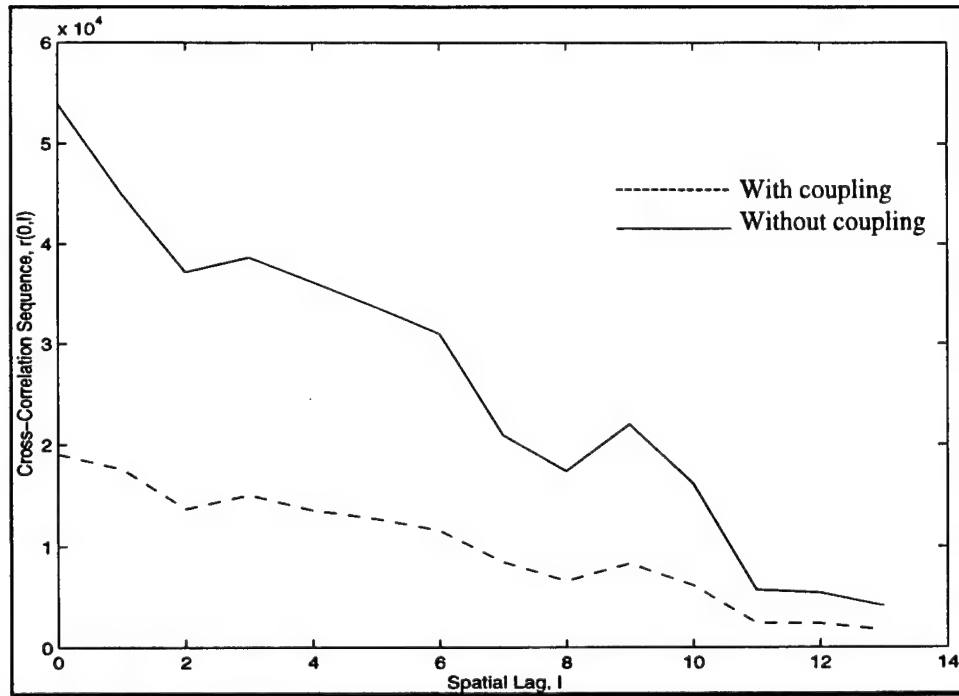


Figure 8. Real part of spatial sample covariance sequence.

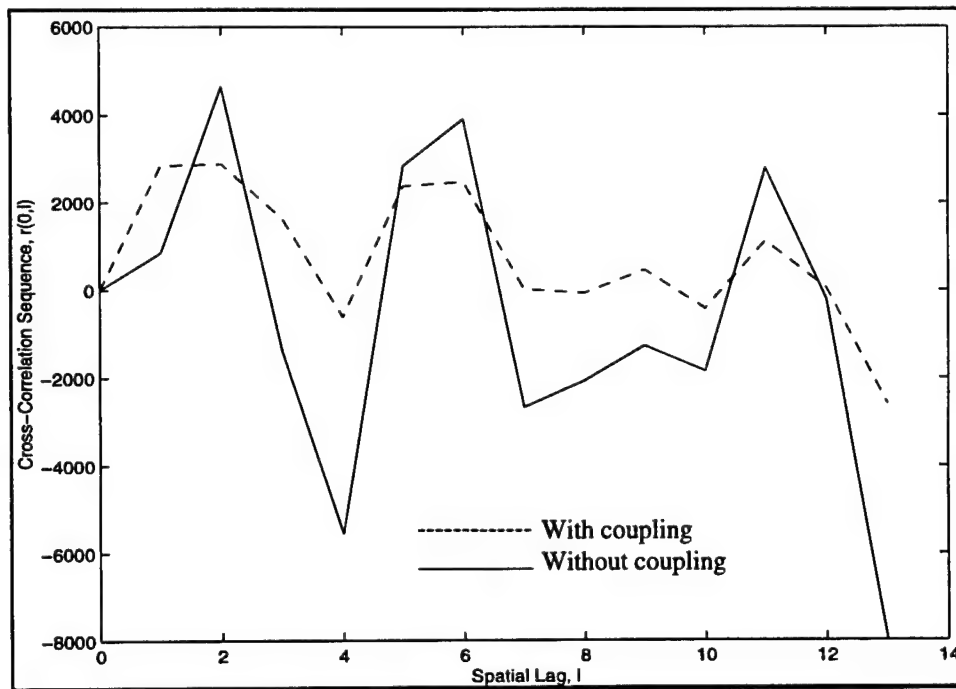


Figure 9. Imaginary part of spatial sample covariance sequence.

Again, the same effects are observed in this case.

The next set of figures shows both the true power spectrum and that obtained through the estimated sample covariance matrix, without mutual coupling first and then with mutual coupling included.

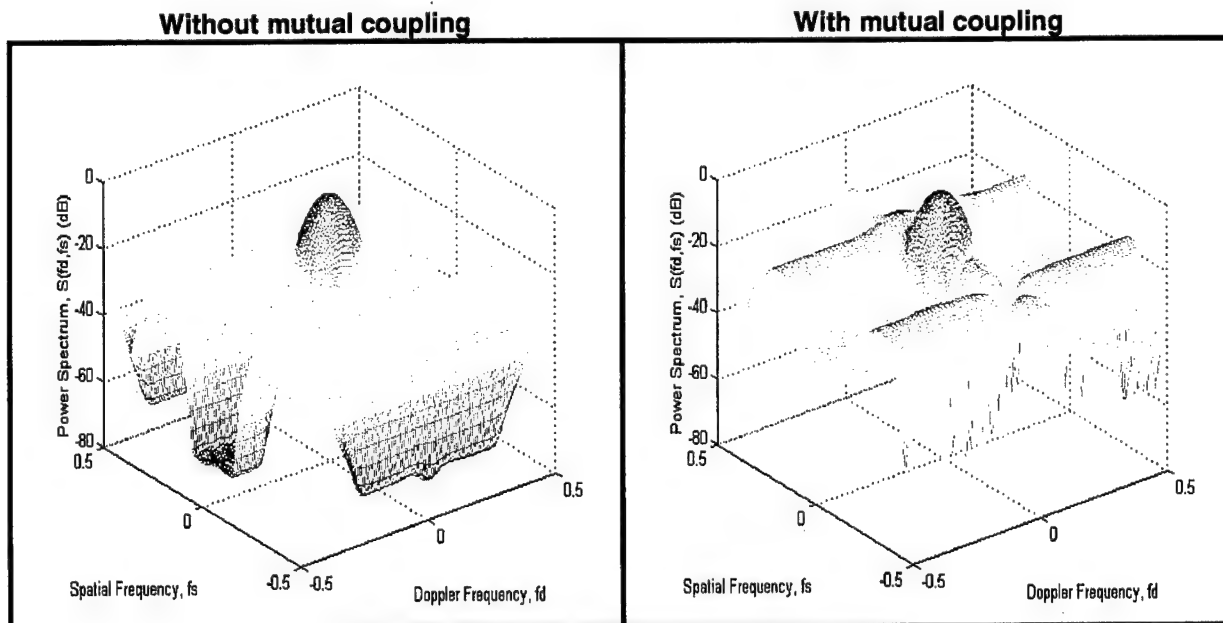


Figure 10. Normalized true power spectrum.

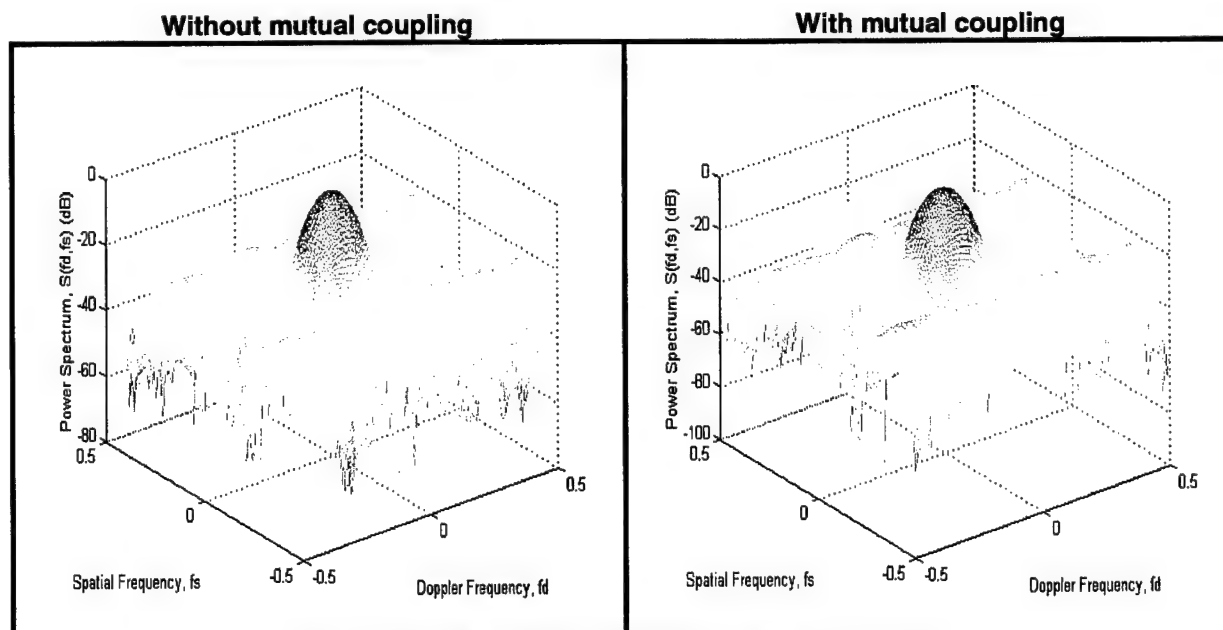


Figure 11. Normalized estimated power spectrum.

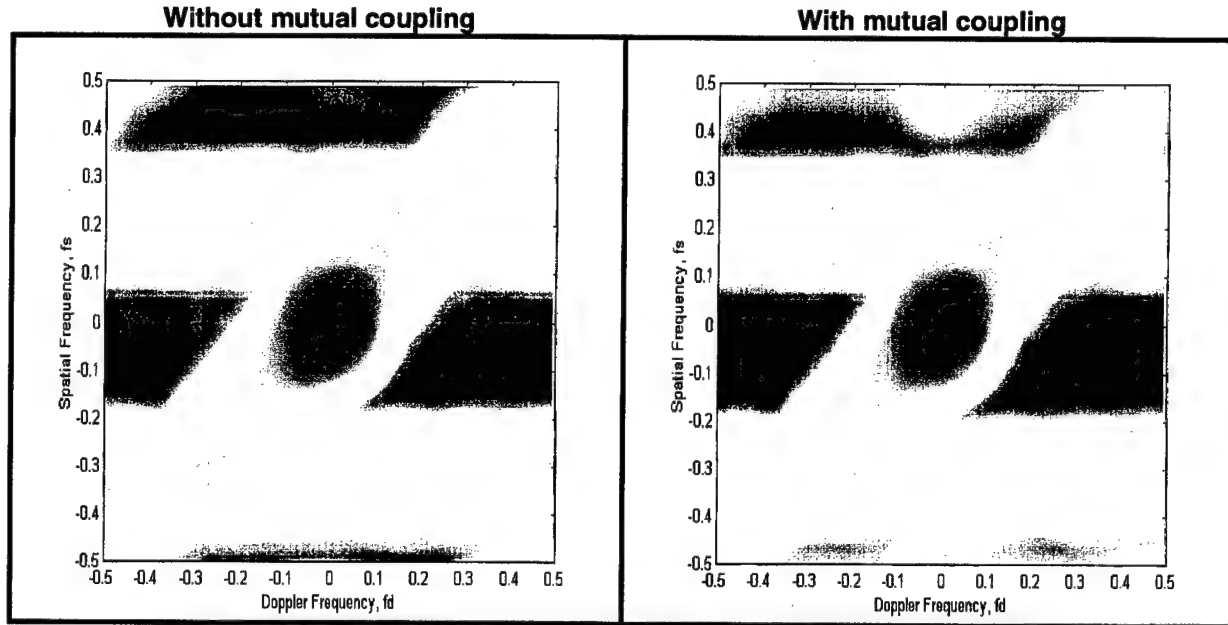


Figure 12. Normalized true power spectrum (modified periodogram).

Note from Figures 10-12 that mutual coupling does change the respective power spectra. In particular, it can be seen from figure 10 that the angle-Doppler map has noticeably changed when mutual coupling is present. Mutual coupling introduces a strong ridge across the spatial frequency domain at zero Doppler. Note also from figure 11 that a strong ridge appears at zero Doppler. The same effect is also seen in figure 12.

4. Application to Space Time Adaptive Processing

In section 3, we included the effects of mutual coupling into the physical model of the MCSPS, from which data is generated for future processing. We have shown how mutual coupling changes the received signals as well as their respective covariance matrices. In this section, we apply some well-known STAP algorithms such as the Adaptive Matched Filter (AMF), also referred to as the CFAR-AMF, to determine the effects of mutual coupling on the performance of these algorithms. To achieve this goal, we generate two sets of data. First, only the true space-time covariance matrices are generated. These in turn will be used in the signal processing aspect of the algorithm. Then, a datacube consisting of J channels, N pulses and K range cells is generated. The needed covariance matrices are estimated using this data. We first apply the CFAR-AMF without mutual coupling and determine the

performance of the algorithm in these conditions. The metrics used to determine the performance of the algorithm are the output SINR and the adapted antenna beam pattern, both plotted as a function of angle and Doppler.

The physical model was modified so that true space-time covariance matrices and a datacube are generated. The covariance matrices have dimension $(JN \times JN)$ and the datacube has dimension $(JN \times K)$. We have successfully been able to generate “true” and “estimated” covariance matrices suitable for STAP processing. This is very practical when performing detection analyses. We programmed the CFAR-AMF approach so that mutual coupling effects will be analyzed. As mentioned earlier, two measures have been used to study the performance of the algorithm, which include the estimated Signal to Interference plus Noise Ratio (SINR) and the adapted beam pattern plotted in the angle-Doppler domain. Both measures were plotted as a function of the steering vectors’ azimuth and Doppler. The estimated SINR tells us how well we have recovered the target after cancellation of the interference, which in turn is best shown by the adapted beam pattern. These are defined as

$$\text{SINR}_{\text{est}} = \frac{|\underline{\mathbf{V}}\underline{\mathbf{R}}^{-1}\underline{\mathbf{X}}^H|^2}{\underline{\mathbf{V}}\underline{\mathbf{R}}^{-1}\underline{\mathbf{V}}^H} \quad (40)$$

and

$$\text{Pat}_{\text{adp}} = \underline{\mathbf{V}}\underline{\mathbf{R}}^{-1}\underline{\mathbf{V}}^H, \quad (41)$$

respectively. Note that the adapted pattern is just the denominator of Equation (40). We have also plotted the variations of the numerator of Equation (40), sometimes referred to as the sample matrix inversion (SMI) test statistic, over angle and Doppler. It is given by

$$\text{SMI} = |\underline{\mathbf{V}}\underline{\mathbf{R}}^{-1}\underline{\mathbf{X}}^H|^2. \quad (42)$$

The scenario, which we ran, was similar to the mountaintop data set [9]. It consists of $J=14$ channels, $N=16$ pulses and $K = 3(JN)=672$ range cells. These will be useful for covariance computation. One target with a signal to noise ratio (SNR) of -5 dB, 361 clutter patches constituting a clutter to noise ratio (CNR) of 38 dB, 2 jammers with a jammer to noise ratio (JNR) of 47 dB have been included in the simulation. The target has a velocity of 33.3 m/s and is located at an azimuthal angle of 0° (mainbeam). This translates into a normalized Doppler frequency of 0.333 and a normalized spatial frequency of zero. Two “true”

covariance matrices, one without mutual coupling and the other with mutual coupling were generated. We also generated two data vectors at the cell under test, one without mutual coupling and the other with mutual coupling. Let \underline{R} , \underline{V} and \underline{X} denote the interference covariance matrix, the steering vector and the data vector, respectively, in the absence of mutual coupling. In the presence of mutual coupling, these quantities are denoted by \underline{R}_z , \underline{V}_z and \underline{X}_z , respectively, where \underline{V}_z is defined below in Equation (43). We have generated three sets of plots. In the first case, no mutual coupling was included. In the second case, mutual coupling is included, however the steering vector in Equations (40)-(42) did not change. In the third case, mutual coupling was included and the steering vector has been replaced by \underline{V}_z . This is shown below.

- Case 1: $\text{SINR}_{\text{est}} = \frac{|\underline{V}\underline{R}^{-1}\underline{X}^H|^2}{\underline{V}\underline{R}^{-1}\underline{V}^H}$, $\text{Pat}_{\text{adp}} = \underline{V}\underline{R}^{-1}\underline{V}^H$ and $\text{SMI} = |\underline{V}\underline{R}^{-1}\underline{X}^H|^2$
- Case 2: $\text{SINR}_{\text{est}} = \frac{|\underline{V}\underline{R}_z^{-1}\underline{X}_z^H|^2}{\underline{V}\underline{R}_z^{-1}\underline{V}^H}$, $\text{Pat}_{\text{adp}} = \underline{V}\underline{R}_z^{-1}\underline{V}^H$ and $\text{SMI} = |\underline{V}\underline{R}_z^{-1}\underline{X}_z^H|^2$
- Case 3: $\text{SINR}_{\text{est}} = \frac{|\underline{V}_z\underline{R}_z^{-1}\underline{X}_z^H|^2}{\underline{V}_z\underline{R}_z^{-1}\underline{V}_z^H}$, $\text{Pat}_{\text{adp}} = \underline{V}_z\underline{R}_z^{-1}\underline{V}_z^H$ and $\text{SMI} = |\underline{V}_z\underline{R}_z^{-1}\underline{X}_z^H|^2$.

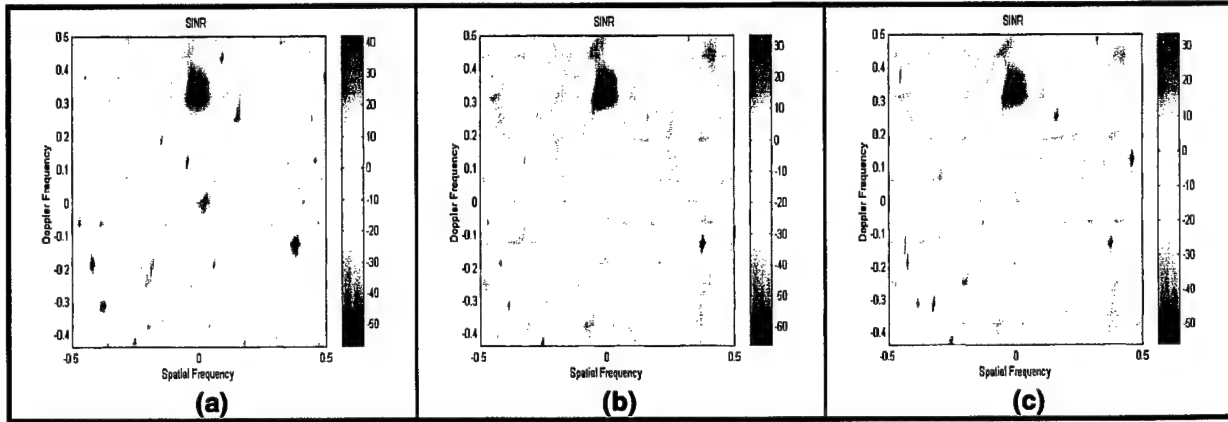


Figure 13. Estimated SINR, (a) without mutual coupling, (b) with mutual coupling, and (c) with compensating for mutual coupling.

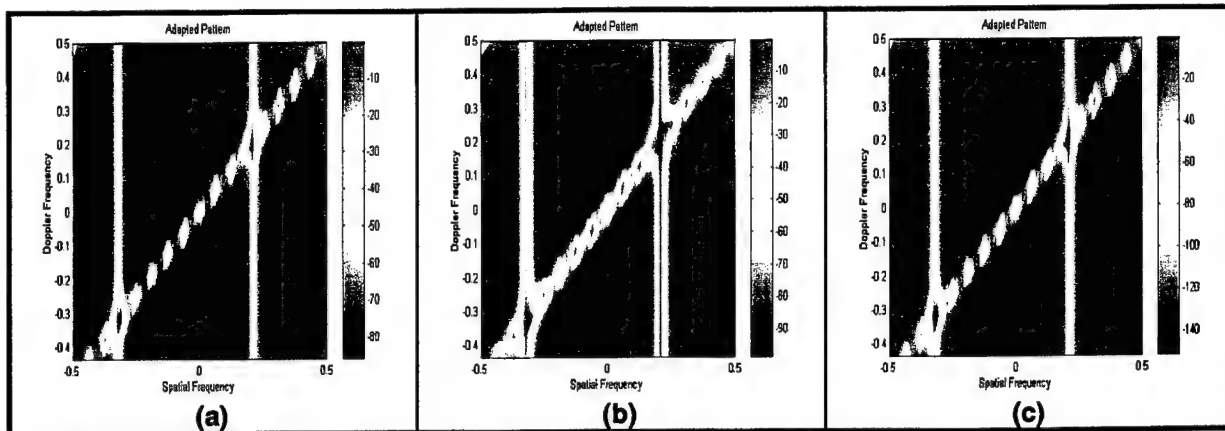


Figure 14. Adapted beam pattern, (a) without mutual coupling, (b) with mutual coupling, and (c) with compensating for mutual coupling.

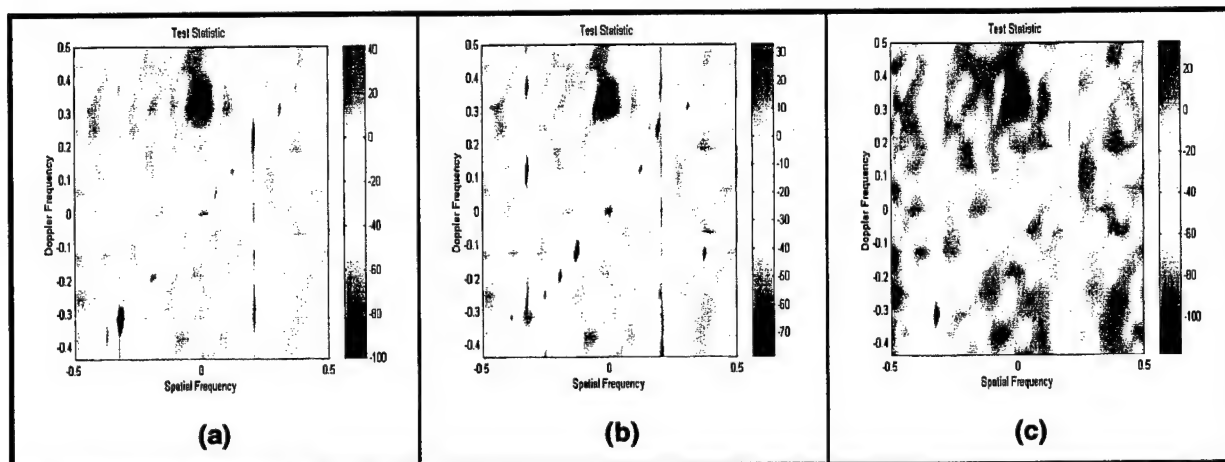


Figure 15. Test statistic, (a) without mutual coupling, (b) with mutual coupling, and (c) with compensating for mutual coupling.

In the ideal case, (Figures 13-15, case (a)), where no mutual coupling was assumed, the CFAR-AMF processor clearly distinguishes the target and cancels the interference. A sharp peak is generated at the location of the target, and two nulls have been generated at the locations of the jammer and a null is generated along the clutter ridge. When mutual coupling was involved, and using ideal steering vectors, (Figures 13-15, case (b)), the target is completely buried. It is extremely difficult to identify the target, even though appropriate nulls have been generated at the jammer locations and along the clutter ridge. The only difference is that the nulls are broader and less deep. This clearly shows that mutual coupling degrades the performance of the CFAR-AMF. Therefore, appropriate measures

have to be developed so as to compensate for these effects. At this stage, our compensating scheme consists of applying steering vectors corrupted with mutual coupling. As discussed earlier, the new steering vector has the form

$$\underline{V}_z = \Gamma \underline{V}, \quad (43)$$

where \underline{V} is the ideal steering vector and Γ is the following matrix

$$\Gamma = \begin{bmatrix} H^{-1} & 0 & \dots & 0 \\ 0 & H^{-1} & \dots & 0 \\ \vdots & \vdots & \ddots & \vdots \\ 0 & 0 & \dots & H^{-1} \end{bmatrix}. \quad (44)$$

Note from Figures (13)-(15), case (c), that this simple compensating scheme worked well in the sense that the target has been recovered better and that the nulls are also clearly distinguished.

The intent of this report was to include the effects of mutual coupling into our simulation capabilities for future analyses regarding their effects on STAP techniques. Future research should be devoted to the study of other sub-optimum techniques. These would include both factored approaches (FTS and FST) [10], the extended factored approach (EFA) [11], adaptive displaced phase center aperture (ADPCA) [12], joint domain localized (JDL) [13], the principal components technique (PC) [14], the cross-spectral metric (CSM) [15] and the newly developed technique termed as the parametric adaptive matched filter (PAMF) [16].

5. Effects of Mutual Coupling on the True SINR

We have also investigated the performance of the sample covariance matrix estimator and compared the performance of the output SINR as a function of number of the sample support size. The output SINR is given by:

$$\text{SINR} = \frac{|\underline{V}^H \hat{R}^{-1} \underline{X}|^2}{\underline{V}^H \hat{R}^{-1} \hat{R} \hat{R}^{-1} \underline{V}}, \quad (45)$$

where R is the true covariance matrix and \hat{R} is the sample covariance matrix estimated using $K = nJN$ secondary data. Note that n is an integer, J is the number of channels and N is the number of pulses.

In the absence of mutual coupling, the following table shows the difference between the true SINR and the estimated SINR as a function of n .

Table 1. SINR as a function of n , no mutual coupling

n	20	60
SINR_t (dB)	28.3572	28.3572
SINR_e (dB)	26.5697	26.5889

In the presence of mutual coupling, the following table shows the difference between the true SINR and the estimated SINR as a function of n .

Table 2. SINR as a function of n , with mutual coupling

n	20	60
SINR_t (dB)	24.2185	24.2185
SINR_e (dB)	22.4393	22.4457

The above tables demonstrate two things:

1. There is a 4 dB difference between the coupled and uncoupled SINR, for both the true and estimated SINR.
2. The estimated SINR approaches the true SINR as n increases.

6. Probability of Detection

In this section, we investigate the effects of mutual coupling on the probability of detection (P_d) of the adaptive CFAR-AMF algorithm for a pre-determined probability of false alarm (P_{fa}). A single target with an SNR of -5dB was assumed. We first checked some prior results from an AFRL in-house analysis conducted by Dr. James Michels. After

conducting validation analyses, the MATLAB codes developed here were optimized to reduce computation run times and were then used to generate probabilities of detection (P_d) curves for several cases, using Monte-Carlo procedures. We noticed significant speedup improvements of the MATLAB code that we implemented. Next, we included the effects of mutual coupling and then computed the corresponding probability of detection.

Figures (16)-(21) show the performance of the CFAR-AMF without and with mutual coupling under different scenarios. The probability of false alarm is kept unchanged for all cases under study and is equal to 0.01 ($P_{fa} = 0.01$). For simplicity and speed up, in the first case, $J = 2$ channels and $N = 2$ pulses have been considered. The results shown below have been generated using 10,000 Monte-Carlo snapshots and averaged over 1000 independent runs.

Figure 16 shows the detection performance of the CFAR-AMF with $K = 1000$ range cells used to estimate the disturbance covariance matrix. The normalized Doppler frequency is assumed to be zero while the elevation and azimuth angles, ϕ and θ , are also assumed to be zero.

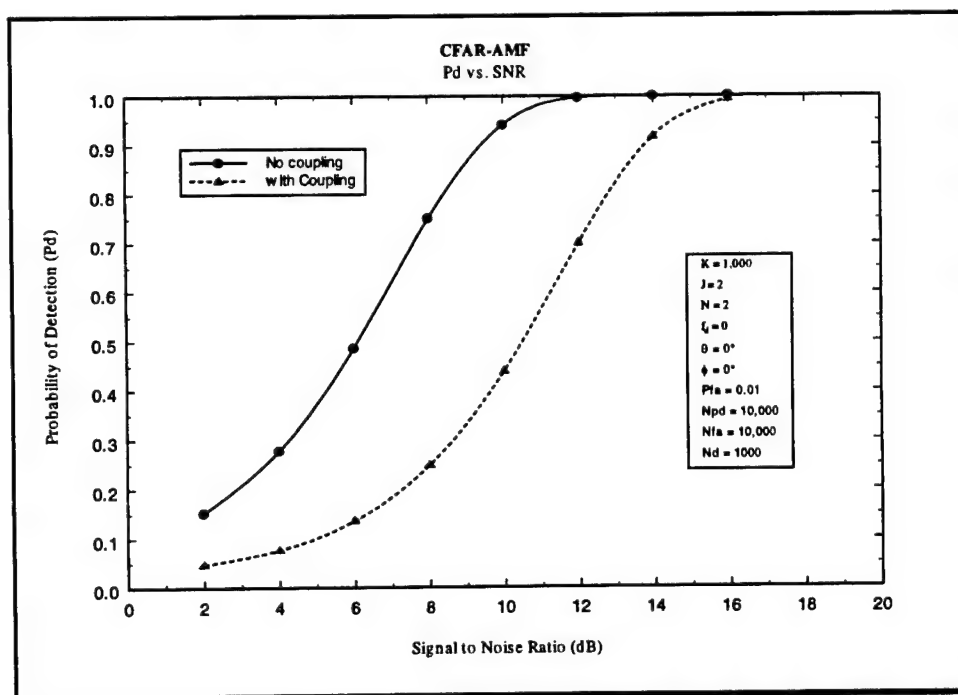


Figure 16. P_d vs. SNR, $K = 1000$.

As can be seen from Figure 16, to achieve the same P_d with and without mutual coupling, an increase of about 5 dB in the signal to noise ratio is needed. This also can be interpreted as having a loss of about 4-5 dB in P_d when mutual coupling is included in the simulation.

Figure 17 is similar to Figure 16. In this case, however, only 8 secondary data vectors have been used for covariance matrix estimation.

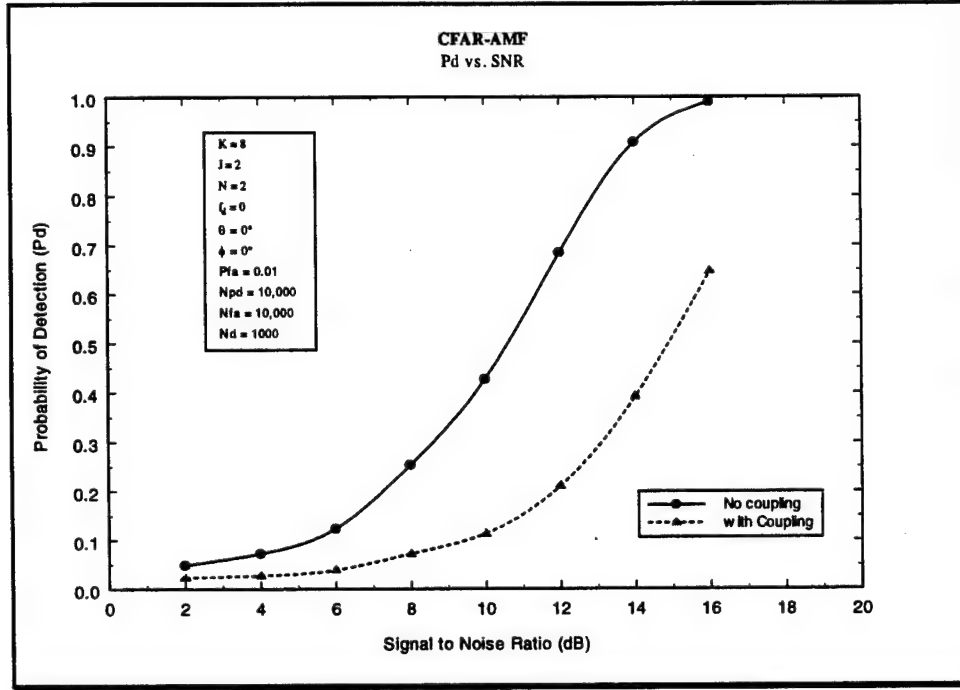


Figure 17. P_d vs. SNR, $K = 8$.

Figure 17 shows very similar P_d behavior as those of figure 16. The only difference is that with $K = 8$, the covariance matrix is estimated with only $2JN$ samples. This is usually the minimum number of samples used. As expected, the performance is lower than with $K=1000$, but the loss in P_d for both cases is the same; i.e.; when mutual coupling is included, there is a 4-5 dB drop in SNR for achieving the same P_d .

Figure 18 shows the variation of P_d as a function of azimuth angle θ of the target, while keeping the SNR, the normalized Doppler frequency and the azimuth angle constant. The Probability of false alarm (P_{fa}) is still kept fixed at 0.01 and $K = 200$ samples are used for covariance matrix estimation. The target was assumed to have an SNR of 10 dB.

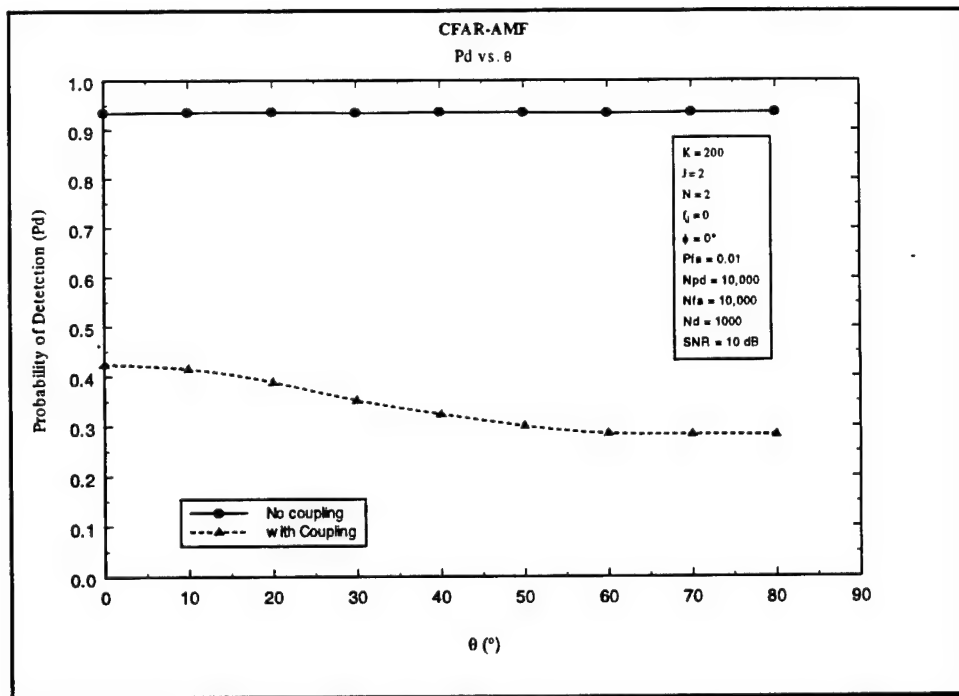


Figure 18. Pd vs. elevation angle θ .

Note from the above figure that Pd drops by more than 50% when mutual coupling is included in the simulation.

Figure 19 shows the variation of Pd vs. the target's normalized frequency. $K = 200$ samples are used for covariance matrix estimation, Pfa was kept at 0.01 and an SNR of 10 dB was assumed. In this case $\theta = 0^\circ$.

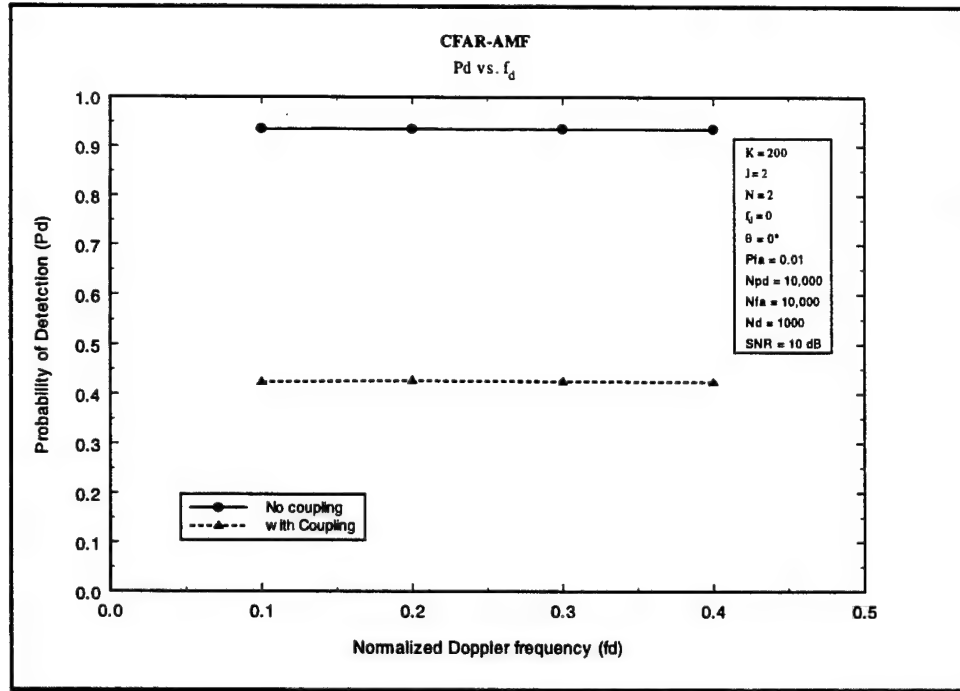


Figure 19. Pd vs. Normalized Doppler Frequency.

Note from the above figure that in the presence of mutual coupling, the probability of detection drops by more than 50%. This is a substantial drop in the performance that should be accounted for when developing schemes to counter mutual coupling.

Figure 20 is similar to Figure 19. The only difference is that $\theta = 30^\circ$.

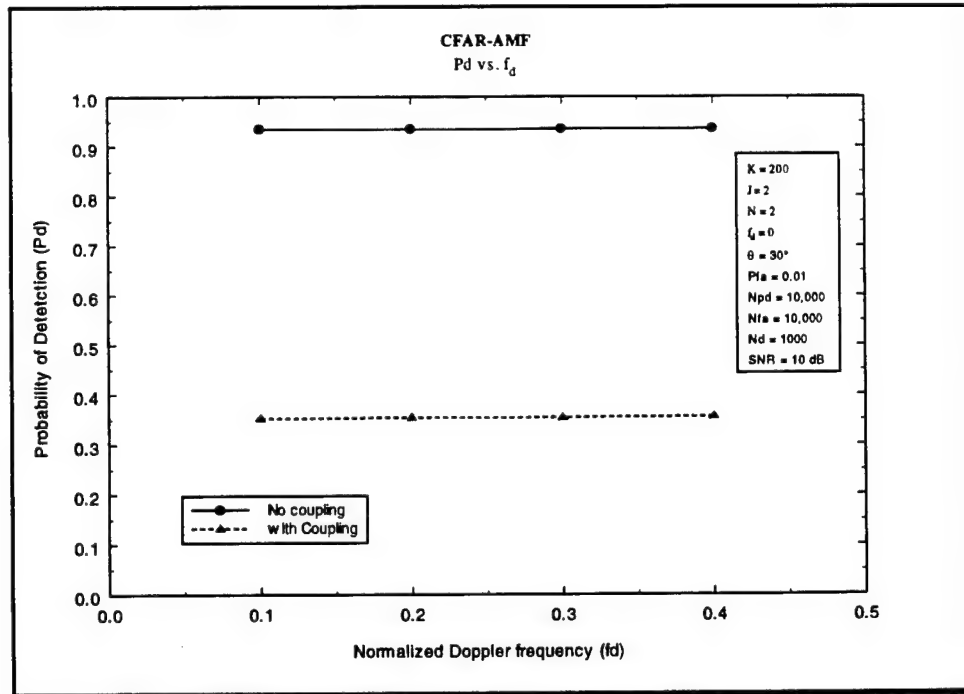


Figure 20. Pd vs. Normalized Doppler Frequency.

The probability of detection drops even further when mutual coupling is present. With mutual coupling present, P_d is constant and is close to 0.36 while it was close to 0.43 when θ was equal to 0° .

Figure 21 is again similar to Figures 19 and 20. In this case $\theta = 60^\circ$.

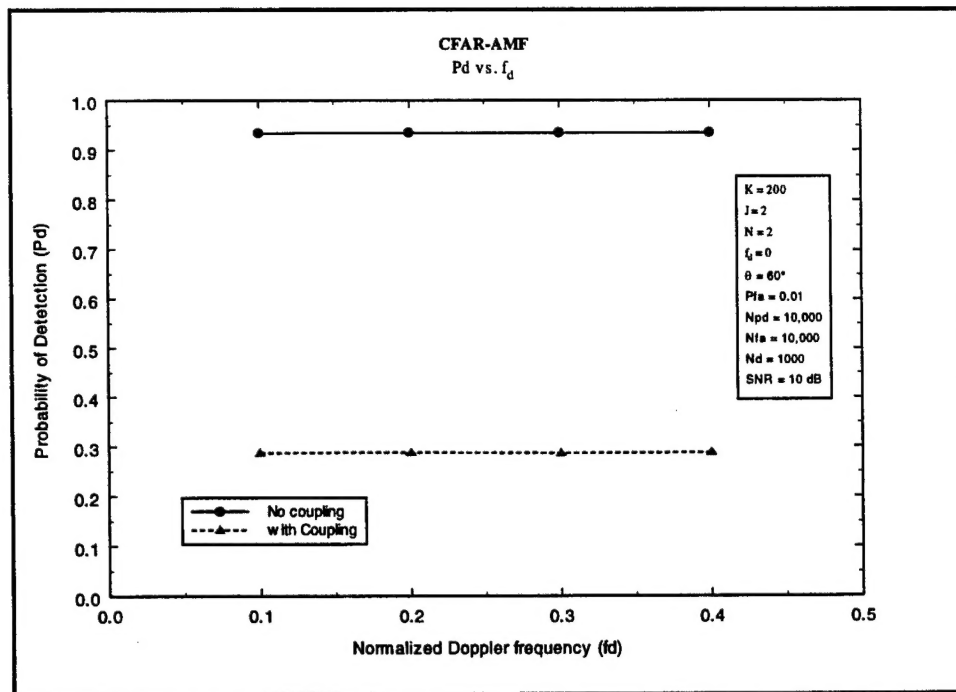


Figure 21. Pd vs. Normalized Doppler Frequency.

In this case the probability of detection is close to 0.29 when mutual coupling is present.

Figure 22 show the performance of the CFAR-AMF without and with mutual coupling in the case where $J = 4$ channels and $N = 8$ pulses. The number of secondary data used is $K = 64$ ($2JN$ criterion). The probability of false alarm is still kept unchanged at 0.01 ($P_{fa} = 0.01$). The results shown below have been generated using 10,000 snapshots and averaged over 1000 runs. The normalized Doppler frequency is assumed to be zero while the elevation and azimuth angles, θ and ϕ , are assumed to be zero.

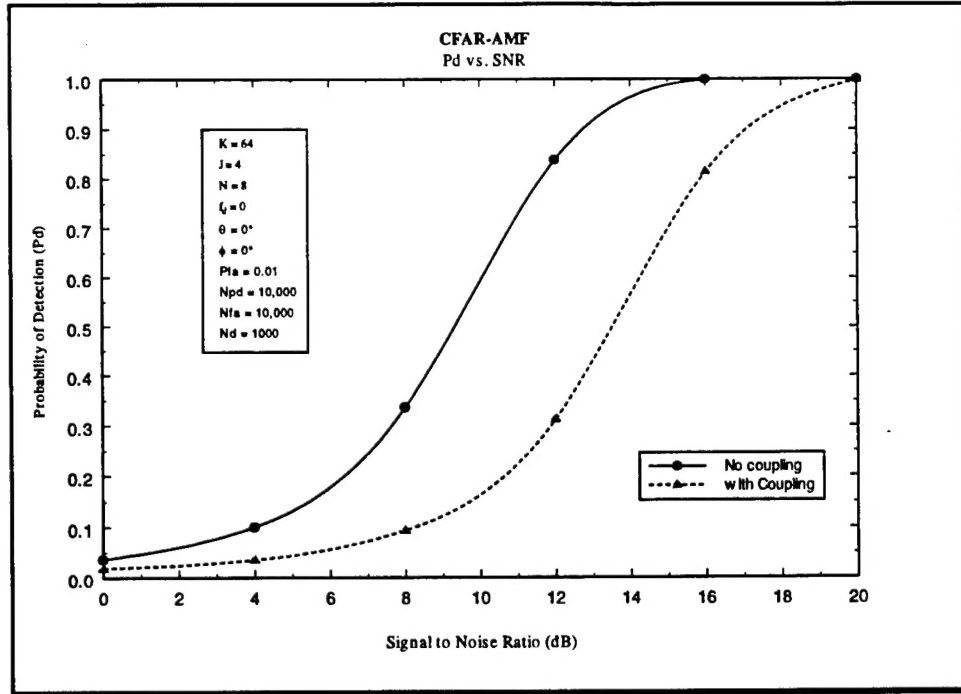


Figure 22. Pd vs. SNR, K = 64.

As can be seen from the above figure, to achieve the same Pd with and without mutual coupling, an increase of about 5 dB in the signal to noise ratio is needed. Therefore, even when J and N are increased to 4 and 8, respectively, the same effect is seen.

7. Conclusions and Recommendations for Future Work

From the above discussions and analyses, it can be concluded that mutual coupling is very important in determining the performance of the AMF. It can be seen that these effects are also geometry depended. We showed that Pd drops by more than 50% depending on the case studied. In some other cases, we showed that in order to achieve the same probability of detection, an increase of about 4 dB in SNR is required. It is our recommendation that close attention should be given to mutual coupling when dealing with space-time adaptive processors. Care should be taken in developing compensation methods so that performance loss is minimized.

References

1. I. J. Gupta and A. A. Ksienski, "Effects of Mutual Coupling on the Performance of adaptive Arrays," IEEE Trans. Antennas and Propagation, Vol. A-P31, No. 5, pp. 785-791, Sept. 1983.
2. C. Yeh and H. L. Leou, "Estimating Angles of Arrival in the Presence of Mutual Coupling," IEEE AP-S Int. Symposium, Vol. 2, pp. 862-865, Blacksburg, VA, 1987.
3. D. H. Shau, "Effects of Mutual Coupling on the Direction Finding Performance of a Linear Array in a Multiple Source Environment using the Method of Moments," Ph.D. dissertation, Syracuse University, May 1988.
4. B. Himed, "Application of the Matrix Pencil Approach to Direction Finding," Ph.D. dissertation, Syracuse University, May 1990.
5. R. F. Harrington, "Field Computation by Moment Methods," Mcmillan, NY 1968.
6. K. M. Pasala and E. M. Friel, "Mutual Coupling Effects and Their reduction in wideband Direction of Arrival Estimation," IEEE Trans. AES, Vol. 30, No. 4, pp.1116-1122, Oct. 94.
7. R. Adve et. al., "Accounting for the Effects of Mutual Coupling in Adaptive Antennas," Proc. 1997 IEEE National Radar Conf., pp.361-366, Syracuse, NY, May 1997.
8. J. R. Roman and D. W. Davis, "Multi-Channel System Identification and Detection Using Output Data Techniques," Rome Laboratory Technical Report, RL-TR-97-5, Vol. II (of two) May 1997.
9. G. W. Titi, "An Overview of the ARPA/Navy Mountaintop Program", In Proc. IEEE Adap. Ant. Systems Symp., Long Island, NY, Nov. 1994.
- *10. A. D. Jaffer et al, "Adaptive Space-Time Processing Techniques for Airborne Radars", Rome Laboratory Technical Report, RL-TR-91-162, July 91.
11. R.C DiPietro, "Extended Factored Space-Time Processing for Airborne Radar", Proc. 26-th Asilomar Conf., Pacific Grove, CA, pp. 425-430, Oct. 92.
12. R. S. Blum et al., 'An Analysis of Adaptive DPCA', Proc. IEEE Natl. Radar Conf., Ann Arbor, MI, pp. 303-308, May 96.
13. H. Wang et al., "On adaptive Spatio-Temporal Processing for Airborne Surveillance Radar Systems", IEEE Trans. AES, Vol. 30, No. 3, pp. 660-670, July 94.
14. A. M. Haimovich, "The Eigencanceller: Adaptive Radar by Eigen-analysis Methods", IEEE Trans. AES, Vol. 32, No. 2, pp. 660-670, April 96.
15. J. S. Goldstein and I. S. Reed, "Subspace Selection for Partially Adaptive Sensor Array Processing", IEEE Trans. AES, Vol. 33, No. 2, pp. 539-544, April 97.
16. J. H. Michels et. al., "Space-Time Adaptive Processing (STAP) in Airborne Radar Applications", IASTED Int. Conf. On Signal Processing and Communications, Canary Islands, Spain, Feb. 11-14 1998.

*RL-TR-91-162 is distribution C1, Limited to U.S. Gov't Agencies and their contractors.

REPRODUCTION QUALITY NOTICE

This document is the best quality available. The copy furnished to DTIC contained pages that may have the following quality problems:

- **Pages smaller or larger than normal.**
- **Pages with background color or light colored printing.**
- **Pages with small type or poor printing; and or**
- **Pages with continuous tone material or color photographs.**

Due to various output media available these conditions may or may not cause poor legibility in the microfiche or hardcopy output you receive.



If this block is checked, the copy furnished to DTIC contained pages with color printing, that when reproduced in Black and White, may change detail of the original copy.